

Characterization of Gamma-irradiated Carbon Nanotube and Metallic Foil Thermal Interface Materials for Space Systems

Robert A. Sayer^{1*}, Stephen L. Hodson^{1,2}, Timothy P. Koehler¹, Robert J. Cordova¹, Timothy C. Marinone¹, Justin R. Serrano¹ and Timothy S. Fisher²

¹Engineering Sciences Center, Sandia National Laboratories, Albuquerque, NM, USA

²School of Mechanical Engineering, Purdue University, West Lafayette, IN, USA

ABSTRACT

Removal of waste heat generated via Joule heating during the operation of electronic devices is critical to overall system performance and reliability. A significant fraction of the overall thermal budget is consumed by heat transfer across the interface of contacting materials. To enhance the flow of heat from source to sink, thermal interface materials (TIMs) are used to reduce thermal contact resistance (TCR) by increasing real contact area at the interface. In space systems, TIMs are exposed to high doses of gamma radiation not encountered in typical terrestrial applications. With typical design lifetimes of 5 years or more, total radiation exposure can be significant and can affect the structure and performance of the TIM. Here, we report measurements of the pressure-dependent TCR of metallic foils and carbon nanotube TIMs (CNT-TIMs) in both vacuum and ambient air environments. The TIMs were irradiated in a gamma cell at a rate of 200 rad/s to a total dose of 50 Mrad. TCR was measured before and after gamma-ray irradiation using a one-dimensional steady-state calorimetric technique at room temperature and contact pressures ranging from 0.5 to 10 MPa. Additionally, the potential for vibration transmission through these interface materials into sensitive electronic equipment is investigated, which is of critical importance during launch when space systems can be subjected to high levels of shock and broad-band vibration. The vibration transmission characteristics of the TIMs were measured from 200 to 4,000 Hz at vibration levels ranging from 1 to 20 g's using an electrodynamic shaker table. CNT-TIMs are shown to exhibit the lowest TCR of any of the tested interface materials, about 38% lower than a plain copper foil. Additionally, all of the TIMs offer little vibration isolation and therefore, care must be taken to isolate sources of vibration that may be transmitted into the electronic components via the TIMs.

1. INTRODUCTION

Heat transfer across the interface of contacting materials is essential to the design and simulation of electronic and thermal systems. When two surfaces are brought into contact, the actual contact area (sum of the contact spot areas) is a small fraction of the apparent area of contact [1]. As a result, heat is restricted to flow through a small number of contact spots formed between the two mating surfaces, which gives rise to a thermal contact resistance (TCR). As a result, TCR can be quite large, causing a large temperature drop across the interface, thus raising the device temperature. Thermal interface

*Corresponding author: E-mail: rsayer@sandia.gov

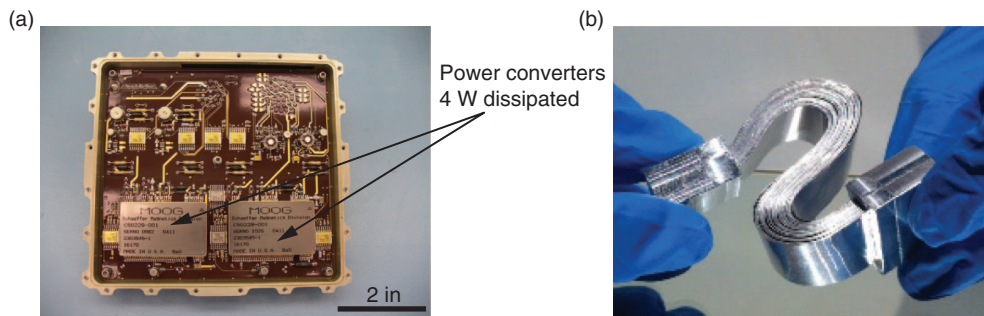


Figure 1. Photographs of (a) a control electronics box and (b) a thermal strap

materials (TIMs) are interstitial materials that are inserted at the contact interface to increase contact area for heat conduction and hence decrease the overall TCR of the joint. Examples of TIMs include common materials such as thermal greases [2], metallic foils [3] and elastomeric sheets [4], and more exotic materials such as conductive polymers [5], carbon nanotubes [6,7] and graphene materials [8,9]. TIMs serve a critical role in thermal management by enhancing heat transfer across contact interfaces, thus allowing higher heat fluxes to be removed from the system and lowering device operating temperature.

Extensive research, primarily driven by the consumer electronics industry, has been conducted to characterize the thermal performance of these various TIMs. However, significant cooling issues exist for military and space applications, which not only require high-reliability cooling solutions, but must also survive harsh environments (vibration and radiation) for extended periods of time (up to 10 years or more) [10]. During the launch of a satellite, for example, the system is subjected to acceleration on the order of ten times the acceleration of gravity, primarily in the frequency range of 500 to 1800 Hz [11]. Although only a couple minutes in duration, this environment causes nearly half of all spacecraft failures [12]. For this reason, vibration isolation systems are put in place to protect the electronics during launch. However, vibration isolation systems are not applied to the thermal straps that connect the electronics to the heat sink (*i.e.* cryo-cooler), and thus can serve as a means of vibration transmission into the electronics boxes. Figure 1(a) shows the interior of a typical control electronics box and Figure 1(b) a thermal strap in which one end would be bolted to the case of the electronics assembly and the other end to the heat sink.

In addition to vibration during launch, space systems are subjected to a wide array of radiation sources including gamma, UV, X-ray, and charged particles—all of which have the potential to drastically affect material properties [13,14] and the structure [15]. UV, X-ray, and charged particles are typically absorbed or reflected by the exterior components of the spacecraft; however, gamma-rays pass through all components with little attenuation, thus affecting the thermal interface material joints in the system. To date, the effect of radiation on thermal performance of mechanical joints has not been well characterized. Here we report measurements of TCR and vibration transmission across both bare joints and joints with thermal interface materials inserted at the contact interface before and after accelerated radiation aging.

2. EXPERIMENTAL METHOD

2.1. Materials

The performance of four different metallic foils including aluminum, copper, nickel and tin (purity greater than 99.5%) as well as a carbon nanotube (CNT) thermal interface material (CNT-TIM) were investigated in this study. The foils were chosen due to their respective variations in material properties summarized in Table 1. Aluminum and copper were chosen due to their high respective thermal conductivities, tin was chosen due to its low hardness, and nickel was chosen due to its combination of low thermal conductivity and high hardness.

Table 1. Material properties of the thermal interface materials

Material	Thermal conductivity (W/mK)	Young's modulus (GPa)	Vickers hardness (MPa)
CNT-TIM	0.5-5	1	–
Aluminum	237	70	167
Copper	401	120	369
Nickel	91	200	638
Tin	67	50	80

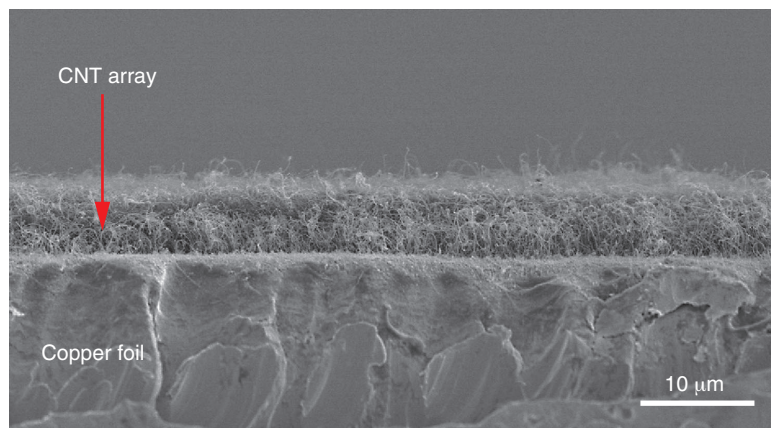


Figure 2. FESEM image of the CNT-TIM

CNT-TIMs were fabricated by growing vertically-aligned multi-walled CNT arrays on both sides of a copper foil. First, a thermal evaporative system was used to deposit a tri-layer metal catalyst stack consisting of 30 nm Ti, 10 nm Al, and 5 nm Fe on both sides of 100 μm thick copper foils. Vertically-aligned CNT arrays were then synthesized in a microwave plasma chemical vapor deposition (MPCVD) system described in detail in Ref. [16]. In summary, the growth chamber was evacuated below 0.15 kPa and purged with N₂ for 5 min. The samples were annealed in N₂ (30 sccm) to a growth temperature of 800°C. The N₂ valve was then closed and 50 sccm of H₂ was introduced to maintain a pressure of 1.3 kPa in the growth chamber. After stabilization of the gas pressure within the chamber, a 300 W plasma was ignited and 10 sccm of CH₄ was introduced as a carbon source to commence 2.5 minutes of CNT synthesis. The samples were imaged using a field-emission scanning electron microscope (FESEM). Figure 2 contains FESEM images of the vertically aligned CNT arrays synthesized on copper foil. The arrays consisted of CNTs with average densities of 10⁸–10⁹ CNTs/mm², nanotube diameters of 30 nm, and lengths of approximately 7 μm.

2.2. Thermal contact resistance measurements

Thermal measurements were conducted using a one-dimensional steady-state conduction technique based upon ASTM standard D5470-06 [17]. The system, shown in Figure 3(a) consists of two 6061 aluminum pillars that serve as heat flow meters (HFMs). Each HFM is 3.8 cm in length, 0.8 cm × 0.8 cm in cross-section, and is instrumented with 6 thermocouples. Linear fits to the temperature data in each HFM are used to determine the heat rate through the test setup and the temperature drop at the interface.

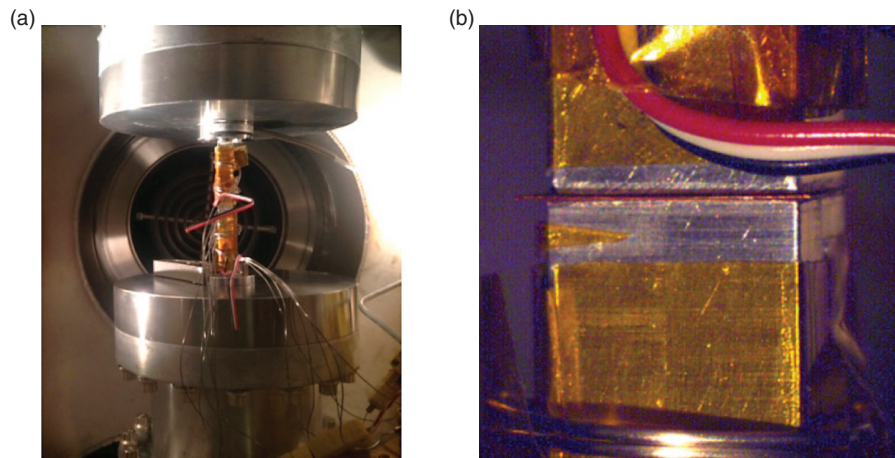


Figure 3. Photographs of (a) the experimental system where the two heat flow meters are placed between a hot plate and cold plate and (b) The contact interface with a 100 μm thick copper foil TIM between the HFMs

The TIM is placed at the interface of the two heat flow meters as shown in Figure 3(b), and the interfacial pressure is adjusted by changing the applied load from two mechanical translators. Interfacial pressures in practice vary by several orders of magnitude depending of the application [18, 19]. Here, the TIMs were tested for interfacial pressure ranging from 0.5 to 10 MPa in order to provide data in the pressure range of many practical space applications [20]. The contact resistance system is housed in a vacuum chamber to eliminate the effects of convection and gas conduction. When a TIM is inserted at the contact interface, the measurement technique yields the overall thermal resistance of the joint, which is a sum of three resistances in series: 1) the contact resistance between the top HFM and the TIM, 2) the bulk thermal resistance of the TIM and 3) the contact resistance between the TIM and the bottom HFM.

2.3. Vibration testing

1 \times 1 in² samples were mounted between a test block and a top plate of the same dimensions and were held together by four #2-56 cap screws as shown in Figure 3. The corners of the TIMs were cut away to not interfere with the cap screws. This setup was chosen as it best represents a heat strap connection, a common application of metallic TIMs in a satellite system. All four screws were tightened to 3 in-lbs to represent a typical applied load for #2 screws. Vibration isolation of the TIMs was characterized in both the normal (*z*-axis) and transverse (*y*-axis) directions. The *x*-direction was not tested due to symmetry between it and the *y*-axis.

2.4. Gamma irradiation

Gamma radiation dose levels can vary greatly by the end of a mission, usually from tens to hundreds of Mrads to the external components of the satellite [21]. Because gamma-rays are high energy and can pass through materials with little attenuation in intensity, similar doses are expected at the interior components of the satellite. Accelerated gamma radiation dosing of the TIM samples was conducted in a ⁶⁰Co gamma cell at a rate of 200 rad/s to a total dose of 50 Mrad in order to simulate a 5 year design life assuming a dose rate of 10 Mrad/yr [21]. For the irradiation process, it is assumed that any gamma induced changes in the material properties will depend on the total dose, but are independent of dose rate [15]. In order to minimize thermal effects during irradiation, the samples were actively cooled and maintained at 297 K.

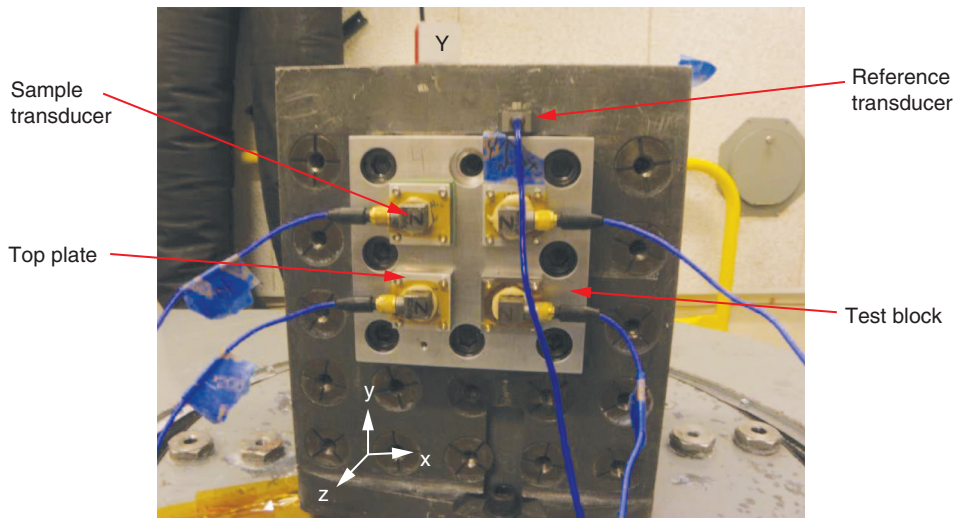


Figure 4. Photograph of the vibration test setup mounted to the shaker

3. RESULTS

The thermal contact resistance of a total of nine different TIMs and a bare aluminum interface, as listed in table 2, was measured for interfacial pressures ranging from 0.5 to 10 MPa. The results of the tests conducted in air and under vacuum are shown in Figure 5.

Figure 5(a) shows that the aluminum, copper, tin and CNT TIMs all offer improved contact resistance in comparison to the bare joint, which are similar to the trends reported by Peterson and Fletcher [3]. In contrast, the joint resistance increases when the nickel foil TIM is used due to its combination of relatively low thermal conductivity and high hardness. The two important material properties in reducing TCR are the mechanical hardness and thermal conductivity of the TIM. Hardness affects the compression of the TIM; softer materials deform more easily than harder materials, and thus can better conform to the rough interface, creating a greater contact area at the interface. On the other hand, thermal conductivity affects both the contact resistance between the TIM and the metallic pillars as well as the bulk resistance of the TIM. Materials with higher thermal conductivity values permit heat to transfer through the bulk with less resistance in comparison to materials with lower thermal conductivity. In addition, the constriction resistance through the contact spots is less for materials with higher values of thermal conductivity. As shown in Table 1, nickel has both low thermal conductivity and high hardness in comparison to the aluminum HFMs, and therefore the increase in TCR is not unexpected.

To explore the effectiveness of the TIMs, consider the results in air at a single interfacial pressure, 6.2 MPa. The TCR of each sample at this pressure is shown in Figure 6. Uncertainty represents the 95% confidence intervals associated with the measurements calculated via a bootstrapping technique [22,23]. At this interfacial pressure, the TCR of the bare interface is 104 mm²K/W. The 25 μm aluminum foil offers very little improvement, reducing the TCR to 101 mm²K/W. The thicker, 100 μm,

Table 2. Summary of the tested TIMs

Sample	1	2	3	4	5	6	7	8	9
Material	Al	Al	Cu	Ni	Ni	Sn	Sn	CNT	bare
Thickness (μm)	25	100	100	25	100	25	100	~120	—

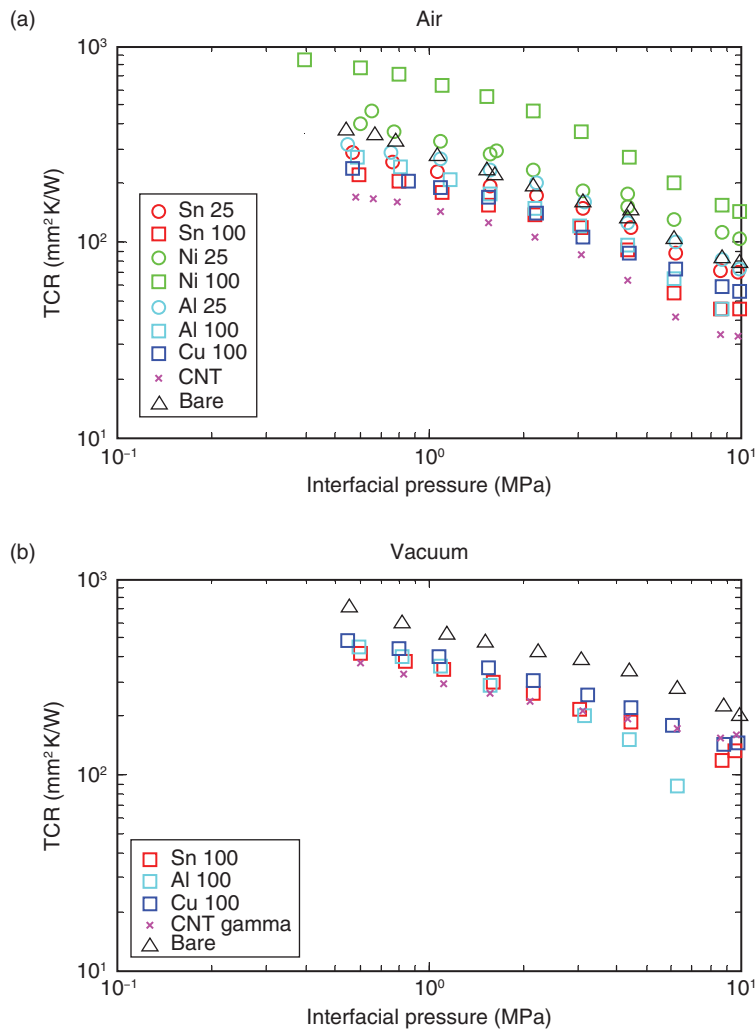


Figure 5. Thermal contact resistance of the tested TIM materials in comparison to the bare aluminum interface in both (a) air and (b) vacuum. (The number after the element name represents the thickness of the foil in micrometers.)

aluminum foil provides a lower TCR ($65 \text{ mm}^2\text{K/W}$) in comparison to the thinner foil. Similar results are shown for the tin foil, which has TCRs of $87 \text{ mm}^2\text{K/W}$ and $55 \text{ mm}^2\text{K/W}$, for the $25 \mu\text{m}$ and $100 \mu\text{m}$ thick foils, respectively. The $100 \mu\text{m}$ copper foil, exhibiting a TCR of $72 \text{ mm}^2\text{K/W}$, offers slightly degraded performance compared to aluminum and tin of equal thickness. This is attributed to the greater hardness of the copper foil, which seems to be the most important parameter in thermal performance. At $42 \text{ mm}^2\text{K/W}$, the CNT-TIM offers the best improvement (more than a factor of two compared to a bare interface) in joint TCR. The nickel foils actually decrease joint conductance. The TCR values of the nickel foils are $131 \text{ mm}^2\text{K/W}$ and $201 \text{ mm}^2\text{K/W}$ for the $25 \mu\text{m}$ and $100 \mu\text{m}$ thick samples, respectively. Here the thinner nickel foil provides lower TCR in comparison to the thicker foil, which is opposite the trend observed for aluminum and tin. This trend was observed by Yovanovich [24], who reported that an optimal foil thickness exists for each metal, which depends on both the composition of the foil and the surface roughness of the joint. Essentially, if the foil is too thin, it does not fill a high percentage of the gaps and if it is too thick it acts more as a solid surface and fails to fill the gaps.

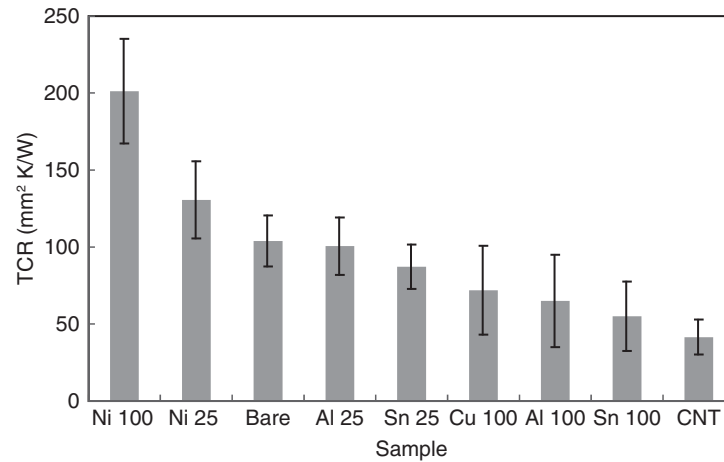


Figure 6. TCR values in air at an interfacial pressure of 6.2 MPa

Figure 7 compares the contact resistance of the TIMs in air and vacuum. When the samples are placed in vacuum, TCR is a factor of 2 to 3 greater in comparison to an air ambient environment. In vacuum, heat transfer is solely due to conduction through solid contact spots. In air, heat can not only flow through the solid spots, but can also conduct across the gas that fills the gaps between the contacting surfaces [25]. Although the thermal conductivity of air is quite low, the large area over which gas conduction can occur enables gas conduction to play a critical role in overall interface conductance.

The effect of gamma irradiation on the thermal performance of the CNT [Figure 7(a)], copper [Figure 7(c)] and nickel [Figure 7(d)] TIMs is also shown in Figure 7. Very little change in TCR of the nickel foil is observed with gamma irradiation. On the other hand, an increase in TCR is observed for the copper foil. In air, as the contact pressure increases, so does the difference in TCR between the radiation-aged and un-aged samples. This increase in TCR is attributed to an increase in hardness of the copper due to gamma radiation [13,14]. For the CNT-TIM at interfacial pressures below 1 MPa, the thermal performance appears to be unaffected by gamma irradiation. However, above 1 MPa, an increase in TCR is observed in the radiation aged sample. This behavior may be explained by the compression of the CNT-TIM. Below 1 MPa, the majority of the deformation is assumed to take place in the CNT array. Because CNTs are inherently thermally radiation hardened, there is no change to the TCR [7]. Above 1 MPa, the TCR of the CNT-TIM follows a trend similar to the 100 μm copper foil. At these pressures, it is likely that the CNT array has been fully compressed and deformation of the copper foil substrate dominates the mechanical behavior of the TIM.

Raman spectroscopy can serve as a valuable method to quantify the quality of CNTs. As photons are absorbed by CNTs, information regarding the amount of disorder, graphitization, and finite size effects are released and measured by the detector. The G-band feature ($\sim 1585\text{ cm}^{-1}$) is associated with the E_{2g} optical phonon modes in graphene and represents the amount of graphitization while the D-peak ($\sim 1360\text{ cm}^{-1}$) is related to vibrational modes associated with the edges of the graphene structure and therefore its presence indicates disorder [26]. The less pronounced D' peak ($\sim 1620\text{ cm}^{-1}$) is related to finite-size effects in the CNT [27]. When analyzing CNTs with Raman spectroscopy, it is common to define the quality of the CNTs using the ratio of the D peak to the G peak as an indicator of long range order in the lattice structure [26]. Therefore, we adopted this metric to evaluate the impact of radiation damage to the CNTs by monitoring the D and G peaks before and after irradiation. A high quality structure will exhibit a lower ratio as the amount of graphitization greatly counter balances the amount of disorder.

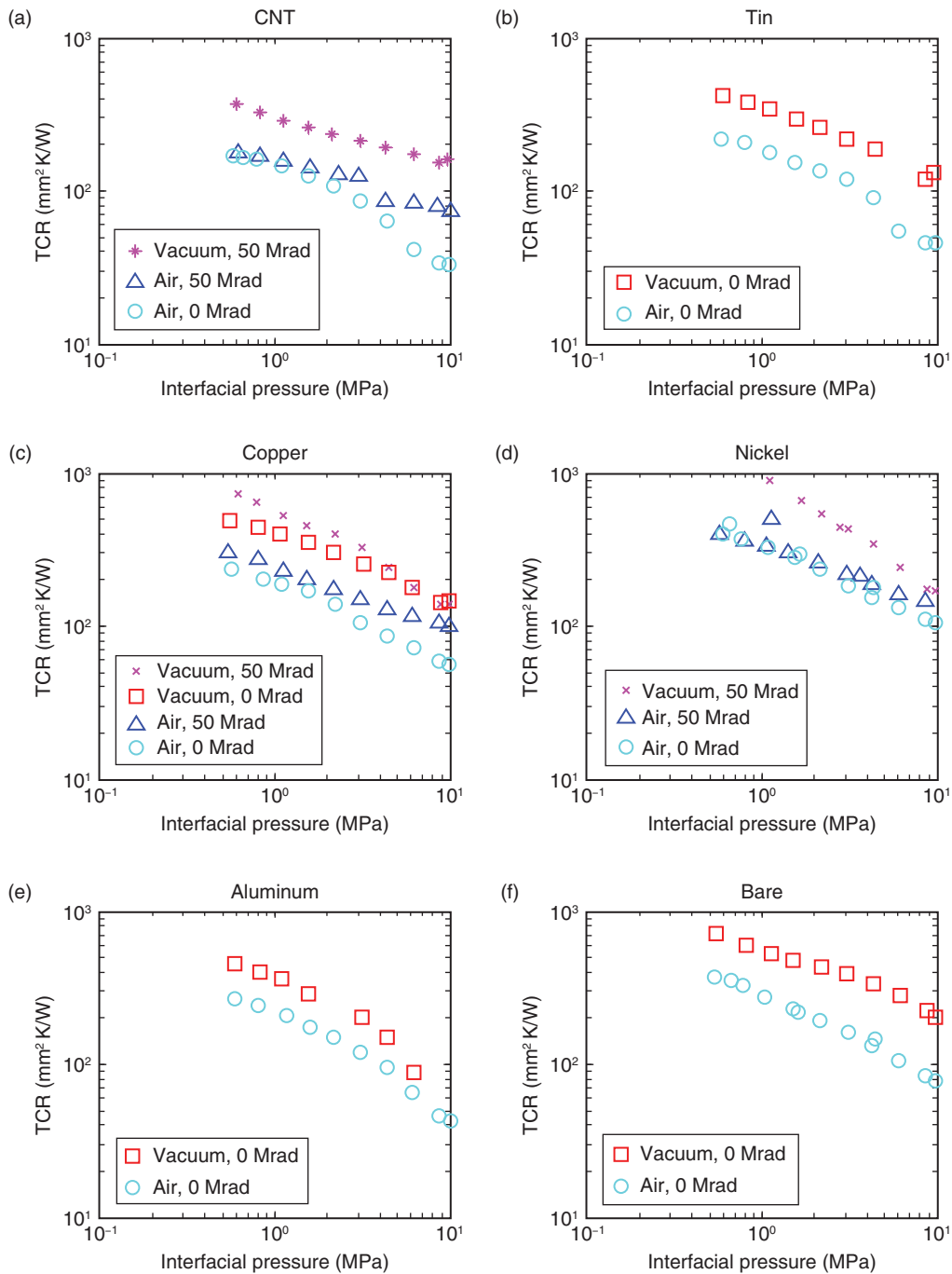


Figure 7. Measured TCR of the (a) CNT, (b) 100 μm tin, (c) 100 μm copper, (d) 25 μm nickel, (e) 100 μm aluminum TIMs, and (f) the bare interface in vacuum and ambient air environments. The effect of gamma irradiation is also shown for the CNT, copper and nickel TIMs

Raman spectra for CNT-TIM samples were collected at several locations on the sample surface before and after exposure to gamma irradiation. The spectra are shown below in Figure 8 and exhibit distinct D and G peaks along with a minute D' peak.

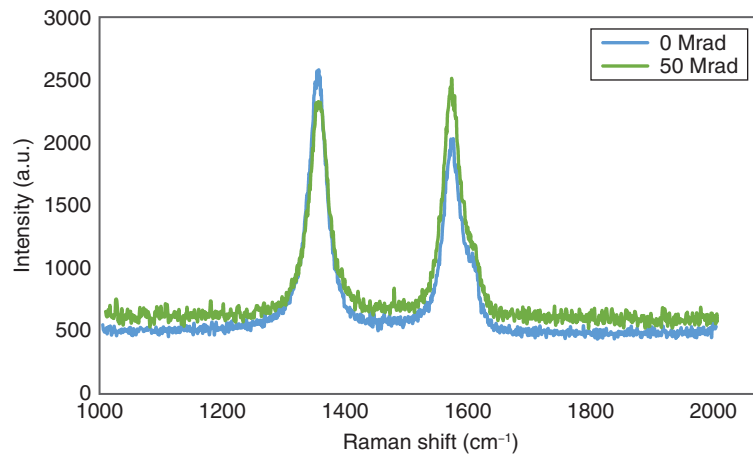


Figure 8. Raman spectra for CNT TIMs before and after exposure to 50 Mrad gamma irradiation

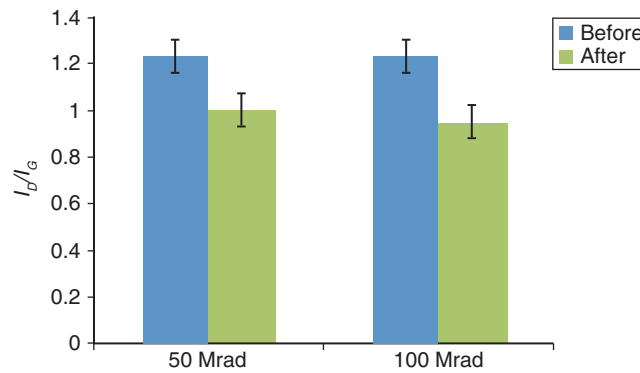


Figure 9. I_D/I_G band ratios for CNT TIMs before and after exposure to 50 and 100 Mrad

The acquired Raman spectra were analyzed by fitting them to a Breit-Wagner-Fano (BWF) spectral line shape [28] which removes uncertainty due to contributions from overlapping peaks when determining the peak intensity. All samples before irradiation showed I_D/I_G ratios of ~ 1.3 which is higher than typical multi-walled CNTs (MWCNTs) [29] indicating significant presence of defects or edge effects resulting from the probing geometry used for the Raman measurement. After irradiation, samples subjected to a 50 Mrad dose exhibited a much lower I_D/I_G ratio of approximately 1.00; 100 Mrad samples showed a slightly lower ratio of approximately 0.95. The ratio of the D'-peak height to the G-peak height is also affected, but less markedly, changing from approximately 0.40 before irradiation to approximately 0.35 after irradiation for both doses. These changes result in a decrease of approximately 20% in the I_D/I_G ratios for both exposures and indicate that the I_D/I_G ratio is marginally dependent on gamma radiation dose, at least within the range of dosages tested. Xu *et al.* [30] reported an increase in graphitic order (8%) of MWCNTs after exposure to 20 Mrad of gamma radiation while Guo *et al.* [31] observed an increase in defect concentration in MWCNTs after exposure within the range of 5 to 25 Mrad of gamma radiation. While their observations are contradicting, the scatter in the reported results can be attributed to the myriad of CNT synthesis techniques that yield different tube structures. As a result, we attribute the increase in quality upon exposure to gamma radiation of these carbon nanotubes to improved graphitization as well as the suppression of additional defects induced by sp^3 hybridization. Figure 9 summarizes these observations. It is noteworthy that although a change in CNT quality is observed, gamma irradiation has little effect on the thermal performance of the CNT-TIM. This is most likely due to offsetting changes in the thermal conductivity and mechanical hardness

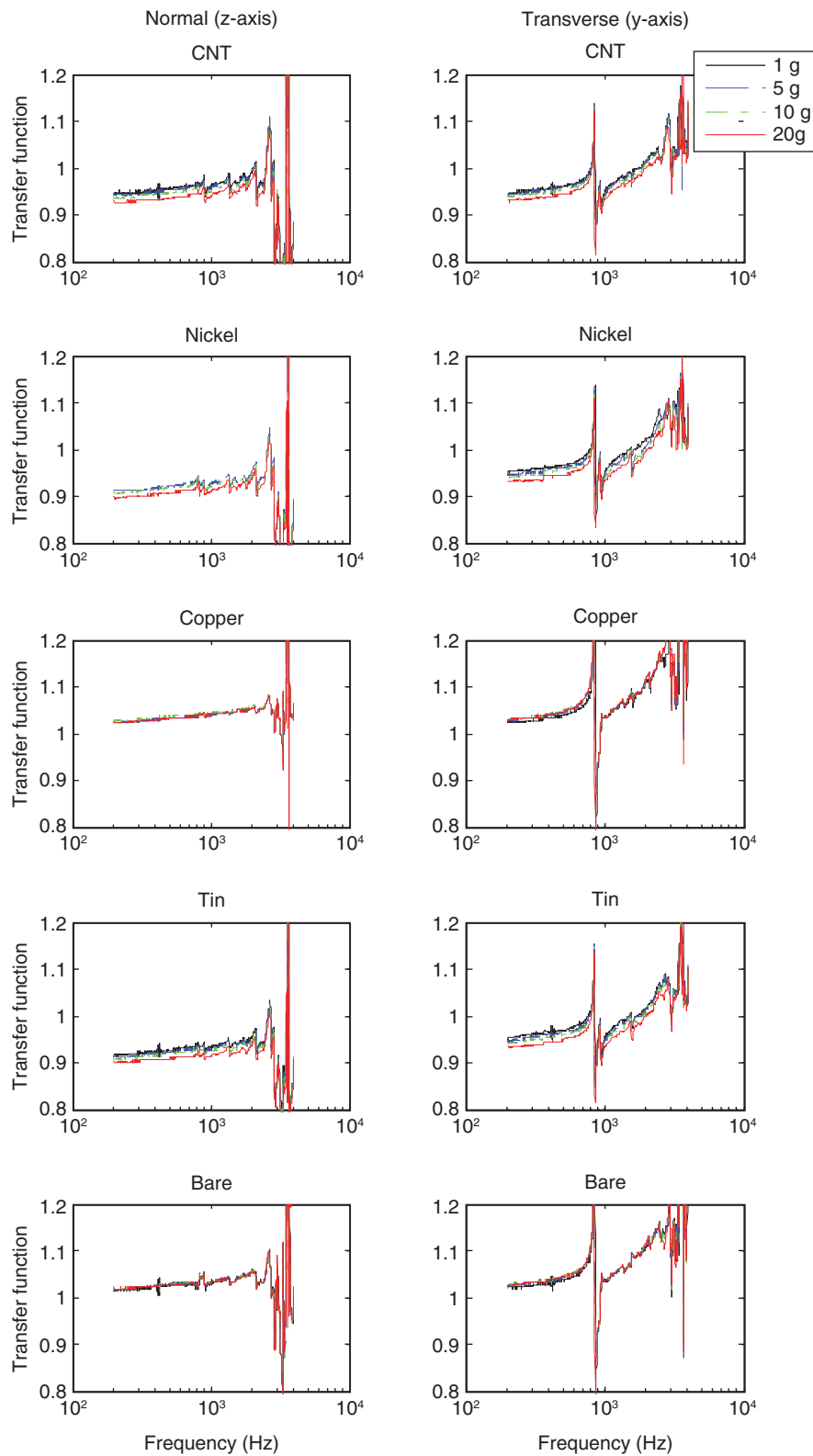


Figure 10. Transfer function from 200 to 4000 Hz for the TIM and bare interface samples at accelerations of 1, 5, 10, and 20 g's. All metallic foils are 100 μm thick. The tightening torque was 3 in-lb.

of the array.

The transmission of vibrations across the contact interface was measured in both the normal and transverse directions for the unaged samples to determine the potential for vibration transmission into the electronics boxes during launch. The results are shown in Figure 10 for acceleration levels of 1, 5, 10 and 20 g's. Here, the transfer function represents the ratio of vibration transmitted across the interface to that of the reference transducer. The vibrational modes of the system occur at the peaks in the figure and are highly dependent on the experimental setup. Significant changes in modes could be observed with any design changes to the setup. Here, the vibrational modes are that from the overall combination of the test block, TIM/bolts, top plate and sample transducer. The first modes occur at 2650 Hz in the normal direction and 840 Hz in the transverse direction. The transfer function at frequencies well below the first mode can be attributed solely to transmission across the interface. This occurs at frequencies below 2000 Hz and 600 Hz in the normal and transverse directions, respectively. At frequencies above the first mode, the transfer function will be a function of both transmission across the interface and amplification due to the natural frequency. These results are highly dependent upon the arrangement of the test apparatus. For example, vibrational modes were measured for the test block at 1890, 3560, 3670 and 3810 Hz. These are a function of the test block geometry and the mounting of the test block to the shaker table. At frequencies below the system modes, the transfer function was approximately 1, which signifies the non-setup dependent response region.

In the low frequency regions, the CNT-TIM and nickel and tin foils provide slight attenuation (5-10%) while slight amplification (3-5%) is found across the copper foil and bare interface. Additionally, the magnitude of transmission across the interface is approximately linear with respect to input acceleration. These results signify that the interface materials do not adequately prevent the transmission of vibration across the bolted interface. As a result, any vibration that is not attenuated in the flexible thermal straps will be transmitted to the electronics control box. This serves as a potential bypass around the vibration isolation systems (damping factors less than 0.01) designed to isolate these systems during launch.

4. CONCLUSION

The thermal contact resistance of carbon nanotube and metallic foil TIMs were measured in comparison to a bare aluminum interface. It is shown that hardness is a critical parameter in TIM performance, with tin, the softest of the tested foils, exhibiting the lowest TCR of the tested foils, and nickel, the hardest tested foil, exhibiting the greatest TCR. The CNT-TIM, which consisted of a 100 μm thick copper foil with a 10 μm thick vertically-aligned, multi-walled CNT array grown on each side of the foil outperformed all of the foil materials, and thus offers promise as a replacement of metallic foils in satellite system thermal designs. It was additionally shown that the employed cooling solutions, consisting of thermal straps connected from the heat source to heat sink, have the potential to adversely transfer vibration to the electronic components during launch of the system. As a result, the heat sink, in addition to the electronics, should be mounted on an isolation system to prevent damage from shock and vibration loading during launch.

ACKNOWLEDGEMENTS

The authors thank Scot E. Swanson for performing the gamma-irradiation of the samples. Sandia National Laboratories is a multi-program laboratory managed and operated by Sandia Corporation, a wholly owned subsidiary of Lockheed Martin Corporation, for the U.S. Department of Energy's National Nuclear Security Administration under Contract DE-AC04-94AL85000.

REFERENCES

- [1] B. Bhushan, Contact mechanics of rough surfaces in tribology: multiple asperity contact, *Tribol. Lett.* 4 (1998) 1–35.
- [2] H. J. Sauer Jr., C.R. Remington, W. E. Stewart Jr., J. T. Lin, Thermal Contact Conductance with Several Interstitial Materials, in: *Proc. 11th Int. Conf. Therm. Conduct.*, Albuquerque, 1971: pp. 22–23.
- [3] G.P. Peterson, L.S. Fletcher, Measurement of Thermal Contact Conductance in the Presence of Thin

- Metal Foils, in: American Institute of Aeronautics and Astronautics, 1988: p. AIAA Paper 88-0466.
- [4] R.A. Sayer, T.P. Koehler, S.M. Dalton, T.W. Grasser, R.L. Akau, Thermal Contact Conductance of Radiation-Aged Thermal Interface Materials for Space Applications, in: ASME 2013 Summer Heat Transf. Conf., 2013: pp. HT2013-17408.
- [5] R.S. Prasher, J.C. Matayabas, Thermal Contact Resistance of Cured Gel Polymeric Thermal Interface Material, IEEE Trans. Components Packag. Technol. 27 (2004) 702-709. doi:10.1109/TCAPT.2004.838883.
- [6] B.A. Cola, X. Xu, T.S. Fisher, Increased real contact in thermal interfaces: A carbon nanotube/foil material, Appl. Phys. Lett. 90 (2007) 093513. doi:10.1063/1.2644018.
- [7] S.L. Hodson, J.R. Serrano, R.A. Sayer, S.M. Dalton, T.P. Koehler, T.S. Fisher, Effect of Gamma-Ray Irradiation on the Thermal Contact Conductance of Carbon Nanotube Thermal Interface Materials, in: ASME 2013 Int. Mech. Eng. Congr. Expo., 2013: pp. IMECE2013-62773.
- [8] A. Rajabpour, S.M. Vaez Allaei, F. Kowsary, Interface thermal resistance and thermal rectification in hybrid graphene-graphane nanoribbons: A nonequilibrium molecular dynamics study, Appl. Phys. Lett. 99 (2011) 051917. doi:10.1063/1.3622480.
- [9] K.M.F. Shahil, A.A. Balandin, Graphene-multilayer graphene nanocomposites as highly efficient thermal interface materials., Nano Lett. 12 (2012) 861-867. doi:10.1021/nl203906r.
- [10] S. V Garimella, A.S. Fleischer, J.Y. Murthy, A. Keshavarzi, R. Prasher, C. Patel, et al., Thermal Challenges in Next-Generation Electronic Systems, IEEE Trans. Components Packag. Technol. 31 (2008) 801-815. doi:10.1109/TCAPT.2008.2001197.
- [11] C.D. Johnson, P.S. Wilke, Protecting Satellites from the Dynamics of the Launch Environment, AIAA J. (2003) 1-10.
- [12] A.S. Bicoso, C. Johnson, L.P. Davis, D. Aerospace, B. Aye, H. Beach, Need for and benefits of launch vibration isolation, 3045 (n.d.) 14-19.
- [13] M. Celina, Selection and Optimization of Piezoelectric Polyvinylidene Fluoride Polymers for Adaptive Optics in Space Environments, High Perform. Polym. 17 (2005) 575-592. doi:10.1177/0954008305052206.
- [14] G. Markovic, M. Marinovic-Cincovic, V. Jovanovic, S. Samardzija-Jovanovic, J. Budinski-Simendic, The effect of gamma radiation on the ageing of sulfur cured NR/CSM and NBR/CSM rubber blends reinforced by carbon black, Chem. Ind. Chem. Eng. Q. 15 (2009) 291-298. doi:10.2298/CICEQ0904291M.
- [15] D. Hui, M.D. Chipara, Radiation-Induced Modifications in Polymeric Materials, MRS Proc. 851 (2004) NN3.9.1. doi:10.1557/PROC-851-NN3.9.
- [16] M.R. Maschmann, P.B. Amama, A. Goyal, Z. Iqbal, R. Gat, T.S. Fisher, Parametric study of synthesis conditions in plasma-enhanced CVD of high-quality single-walled carbon nanotubes, Carbon N. Y. 44 (2006) 10-18. doi:10.1016/j.carbon.2005.07.027.
- [17] Standard Test Method for Thermal Transmission Properties of Thermally Conductive Electrical Insulation Materials 1, Annu. B. ASTM Stand. 06 (2011) D5470-06. doi:10.1520/D5470-06R11.
- [18] R. Prasher, Thermal Interface Materials: Historical Perspective, Status, and Future Directions, Proc. IEEE. 94 (2006) 1571-1586. doi:10.1109/JPROC.2006.879796.
- [19] M. Tirovic, G.P. Voller, Interface pressure distributions and thermal contact resistance of a bolted joint, Proc. R. Soc. A Math. Phys. Eng. Sci. 461 (2005) 2339-2354. doi:10.1098/rspa.2005.1452.
- [20] C.L. Yeh, C.Y. Wen, Y.F. Chen, S.H. Yeh, C.H. Wu, An experimental investigation of thermal contact conductance across bolted joints, Exp. Therm. Fluid Sci. 25 (2001) 349-357.
- [21] R. Akau, D. Pattison, K. Austin, S. Dalton, C. Ho, Nexus Test Report for Thermal and Mechanical Study of Silver-Teflon Tape for Space Applications, 2012.
- [22] B. Efron, Bootstrap methods: Another look at the jackknife, Ann. Stat. 7 (1979) 1-26.
- [23] B. Efron, R. Tibshirani, Statistical data analysis in the computer age, Science (80-.). 253 (1991)

- 390–395.
- [24] M.M. Yovanovich, Effect of foils on joint resistance: evidence of optimum thickness, in: *AIAA Pap.*, 1972: pp. 227–245.
 - [25] C. V Madhusudana, *Thermal Contact Conductance*, Springer-Verlag, New York, 1996.
 - [26] A.C. Ferrari, J. Robertson, Raman spectroscopy of amorphous, nanostructured, diamond – like carbon, and nanodiamond, (2004). doi:10.1098/rsta.2004.1452.
 - [27] W. Li, H. Zhang, C. Wang, Y. Zhang, L. Xu, K. Zhu, et al., Raman characterization of aligned carbon nanotubes produced by thermal decomposition of hydrocarbon vapor, *Appl. Phys. Lett.* 70 (1997) 2684. doi:10.1063/1.118993.
 - [28] S.D.M. Brown, A. Jorio, P. Corio, M.S. Dresselhaus, G. Dresselhaus, R. Saito, et al., Origin of the Breit-Wigner-Fano lineshape of the tangential G-band feature of metallic carbon nanotubes, *Phys. Rev. B.* 63 (2001) 155414. doi:10.1103/PhysRevB.63.155414.
 - [29] H.M. Heise, R. Kuckuk, A.K. Ojha, A. Srivastava, V. Srivastava, B.P. Asthana, Characterisation of carbonaceous materials using Raman spectroscopy: a comparison of carbon nanotube filters, single- and multi-walled nanotubes, graphitised porous carbon and graphite, *J. Raman Spectrosc.* 40 (2009) 344–353. doi:10.1002/jrs.2120.
 - [30] Z. Xu, L. Chen, L. Liu, X. Wu, L. Chen, Structural changes in multi-walled carbon nanotubes caused by γ -ray irradiation, *Carbon N. Y.* 49 (2011) 350–351. doi:10.1016/j.carbon.2010.09.023.
 - [31] J. Guo, Y. Li, S. Wu, W. Li, The effects of gamma-irradiation dose on chemical modification of multi-walled carbon nanotubes., *Nanotechnology.* 16 (2005) 2385–2388. doi:10.1088/0957-4484/16/10/065.

